Journal of Engineering and Applied Sciences 13 (Special Issue 9): 6927-6933, 2018
ISSN: 1816-949X

Simulation of Flow-Induced Noise in a Circular Orifice Pipe from Broadband Source

Chatpawee Taniteerawong, Supanut Supanundha and Kuntinee Maneeratana
Department of Mechanical Engineering, Faculty of Engineering, Chulalongkorn University, Bangkok, Thailand

Abstract: This research studied the flow induced noise by the CFD program fluent as the first step towards the simulation of snoring. Three verification cases included turbulent flow in pipe and turbulent flow through circular orifice in pipe using axial symmetric domains. The case study on flow induced noise using broadband noise source mode was modeled for acoustic power generated by turbulent flow through circular orifice at 8 air inlet velocities 14, 20, 28, 32, 45, 56, 68 and 75 m/sec. The results were compared with existing experimental data. Acoustic power can be well predicted at the mean velocity range of 32-75 m/sec, this made the model unsuitable for the desired purpose which occurred at a low speed.

Key words: Acoustic, orifice, turbulent flow, finite volume method, acoustic power, Thailand

INTRODUCTION

Snoring has received much medical attention in recent years because it was found that up to 20% of adults snore inveterately (Jennum and Sjol, 1993). The sudden obstruction and reopening of the upper airway were the main cause of snoring. The loud noise not only interrupted bed partner's sleeping but also led to the obstructive sleep apnea syndrome.

The use of computational mechanics had been used to study to confirm the cause of problems as well as suggesting the possible treatment details. For example, the expected predisposition of apneic patients was confirmed and based on the flow characteristics, the severity of symptom could be predicted (Rasani *et al*., 2011a, b). The location of treatment device could be better located. Also, the screening of suitable patients for low success surgery treatment could be more accurately predicted (Mihaescu *et al*., 2008).

The baseline requirement for all successes of these work was the of sufficiently accurately CFD simulation. There were many works on the simulation with different degrees of sophistication. In the broad view, the simulation of snoring was very difficult due to complicate non-linear mathematical models with many unknown variables in the multi-physics setting with high non-linearity in every physical domain (Rasani *et al*., 2011a, b). Usually, only specific sections of the airways were modeled (Sarasaen *et al*., 2012; Wexler *et al*., 2005) but sometimes the model encompassed the whole head (Liu *et al*., 2007).

In view of making an easy simulation procedure, so that, the practitioners with low experiences in computational mechanics could model the problem as a canned step-by-step process while sufficient accuracy was ensured. As it might very difficult and expensive to obtain superlative accurate results of problems for specific cases, simply knowing the trends and impact level of parameter changes would already be very useful as compared to the several practices of relying on experiences.

Hence, the goal of this research specified that the employed model had to have as low a complexity in terms of constitutive relationships and physical domains as possible. However, it must not too simple such that the physical interpretation might not be suitable for modeling flow-induced noises such as an incompressible Newtonian fluid (Sarasaen *et al*., 2012) or simple Navier-stokes equations (Wexler *et al*., 2005). Also, This model would be easier to deploy if it was applicable in a wide range of conditions, ideally covering all the actual ranges.

The first step to obtain such computational model was to investigate possible candidates for practical utilization with utmost care with thorough verification, particularly for the acoustic aspect. This project started with the simulation of noise induced by air flows in a duct using the commercial fluent which utilized the Finite Volume Method (FVM) as the first step towards the goal. In this case, the obvious choice was to add the noise simulation to the air flow and investigate the results for the suitability of the model. It was noted that the flow

Corresponding Author: Chatpawee Taniteerawong, Department of Mechanical Engineering, Faculty of Engineering, Chulalongkorn University, Bangkok, Thailand

model without the acoustic equations had been used for a medical application (Mihaescu *et al*., 2008). Thus, this research studied the noise-induced flow of air in a pipe with orifice which represented the obstacle. The results were found to determine whether the proposed model could yield a sufficient accuracy results in the desired air velocities.

MATERIALS AND METHODS

Governing equations

Turbulent flow model: The ensemble-averaged, Reynolds-Averaged Navier-Stokes (RANS) equations could be written as:

$$\frac{\partial \rho}{\partial t} + \frac{\partial}{\partial x_i}(\rho u_i) = 0 \quad (1)$$

$$\frac{\partial}{\partial t}(\rho u_i) + \frac{\partial}{\partial x_j}(\rho u_i u_j) = -\frac{\partial p}{\partial x_i} + \frac{\partial}{\partial x_j}\left[\mu\left(\frac{\partial u_i}{\partial x_j} + \frac{\partial u_j}{\partial x_i} - \frac{2}{3}\delta_{ij}\frac{\partial u_l}{\partial x_l}\right)\right] + \frac{\partial}{\partial x_j}(-\rho\overline{u}_i\overline{u}_j) \quad (2)$$

Where:

ρ = The density of fluid
u_i = The velocity vector
μ = The fluid viscosity
x_i = The coordinates. RANS equations were the same as the Navier-Stokes equations with the additional Reynolds stress
$-\rho\overline{u}_i, \overline{u}_j$ = To represent the turbulence

The Reynolds stress in Eq. 2 had to be properly modeled. In this study, the standard K-ε turbulence model was used because of its reasonable accuracy for a wide range of turbulent flow. The k-ε Model was based on Boussinesq hypothesis and transport equations for turbulence kinetic energy k and its dissipation rate ε which related the Reynolds stress to mean velocity gradient:

$$-\rho\overline{u}_i\overline{u}_j = \mu_t\left(\frac{\partial u_i}{\partial x_j} + \frac{\partial u_j}{\partial x_i}\right) - \frac{2}{3}\left(\rho k + \mu_t\frac{\partial u_k}{\partial x_k}\right)\delta_{ij} \quad (3)$$

where, turbulence viscosity $\mu_t = \rho C_\mu K^2/\varepsilon$ with constant C_μ. The k and ε comes from:

$$\frac{\partial(\rho k)}{\partial t} + \frac{\partial(\rho k u_i)}{\partial x_i} = \frac{\partial}{\partial x_j}\left[\left(\mu + \frac{\mu_t}{\sigma_k}\right)\frac{\partial k}{\partial x_j}\right] + G_k + G_b + \rho\varepsilon - Y_M + S_k \quad (4)$$

$$\frac{\partial}{\partial t}(\rho\varepsilon) + \frac{\partial}{\partial x_i}(\rho\varepsilon u_i) = \frac{\partial}{\partial x_j}\left[\left(\mu + \frac{\mu_t}{\sigma_\varepsilon}\right)\frac{\partial e}{\partial x_j}\right] + C_{1\varepsilon}\frac{e}{k}(G_k + C_{3e}G_b) - C_{2e}\rho\frac{\varepsilon^2}{k} + S\varepsilon \quad (5)$$

Where:

G_k = Represented the generation of turbulence kinetic energy due to mean velocity gradients
G_b = The generation of turbulence kinetic energy due to buoyancy
Y_M = The contribution of the fluctuating dilatation in compressible turbulence to the overall dissipation rate
S_k and S_ε = Source terms
σ_k and σ_ε = The turbulent Prandtl numbers for k and ε, respectively while $C_{1\varepsilon}$ $C_{2\varepsilon}$ and $C_{3\varepsilon}$ were constants

Aerodynamically generated noise: With the complexity of the aerodynamically generated noise, there were a number of computational approaches. In fluent, there were three methods of computing aerodynamically generated noise: the direct method an integral method that was based on acoustic analogy and the broadband noise source models (Fluent, 2009).

In the direct method, both generation and propagation of sound waves were directly computed by solving the fluid dynamics equations. Sound waves prediction required time-accurate solutions of the governing equations and the compressible fluid flow model was needed.

For the integral method which predicted mid-to far-field noises, the model was based on the Lighthill's acoustic analogy. The important limitation of this model was that it was applicable only to sound in free space.

In the broadband noise source models for practical applications involving turbulent flows, noise did not have any distinct tones and the sound energy was continuously distributed over a broad range of frequencies. Statistical turbulence quantities from RANS equations could be employed with semi-empirical correlations and Lighthill's acoustic analogy.

The broadband noise source models did not require transient solutions to any governing fluid dynamics equations. All required data could be obtained from RANS Models such as the mean velocity field, turbulent kinetic energy k and the dissipation rate ε. Therefore, the use of broadband noise source models required the least computational resources. As a result, this model was selected as the first candidate to study.

The fluent offered several such broadband noise source models, namely, Proudman's formula, jet noise source model, boundary layer noise source model, source terms in the linearized Euler equations and source terms in Lilley's equation.

This research used the jet noise source model because this model was suitable for axisymmetric jets as found in the case study (Van Herpe *et al*., 1995). Acoustic power L_P in dB was computed from:

$$L_p = 10\log\left(P_A/P_{ref}\right) \quad (6)$$

where, the reference acoustic power $P_{ref} = 10^{-12}W/m^2$, P_A was the total acoustic power emitted by the unit volume of axisymmetric turbulence.

Goldstein and Rosenbaum (1973) derived a formula for the total acoustic power emitted by a unit volume of axisymmetric turbulent jet:

$$P_A(\vec{y}) = 2\pi r^2 \int_0^{\pi} I(r,\theta;\vec{y})\sin\theta d\theta \quad (7)$$

where r and θ were the radial and angular coordinates of the receiver location. The I(r, θ; Y) was the directional acoustic intensity per unit volume of a jet defined by:

$$I(r,\theta;\vec{y}) = \frac{12\rho_0\omega_f^4 L_1 L_2^2 \overline{u}_{t1}^{2^2}}{5\pi a_0^5 r^2}\frac{D_{self}}{C^5} + \frac{24\rho_0\omega_f^4 L_1 L_2^4 \overline{u}_{t1}^2}{pa_0^5 r^2}\left(\frac{\partial U}{\partial r}\right)^2\frac{D_{shear}}{C^5} \quad (8)$$

Variables and parameters (Laufer, 1954) could be obtained while the values of $\overline{U}_{f1}^2$ and $\overline{U}_{t2}^2$ depended on the turbulence model used for simulation:

$$C = 1 - M_c\cos\theta \quad (9)$$

$$D_{self} = \frac{1}{3}\left[\frac{M^2}{7} + M - 1.5N\left(3 - 3N + \frac{1.5}{\Delta^2} - \frac{\Delta^2}{2}\right)\right] \sin^4\theta + 1 + 2\left(\frac{M}{9} - N\right)\cos^2\theta\sin^2\theta \quad (10)$$

$$D_{shear} = \cos^2\theta\left[\cos^2\theta + \frac{1}{2}\left(\frac{1}{\Delta^2} - 2N\right)\sin^2\theta\right] \quad (11)$$

$$\Delta = \frac{L_2}{L_1}, M = \left[\frac{3}{2} - \left(\Delta - \frac{1}{\Delta}\right)\right]^2, N = 1 - \frac{\overline{u}_{t2}^2}{\overline{u}_{t1}^2}, L_1 = \frac{\left(\overline{u}_{t1}^2\right)^{3/2}}{e}, L_2 = \frac{\left(\overline{u}_{t2}^2\right)^{3/2}}{\varepsilon}, \omega_f = 2\pi\frac{\varepsilon}{k}, \overline{u}_{t1}^2 = \frac{8}{9}k, \overline{u}_{t2}^2 = \frac{4}{9}k \quad (12)$$

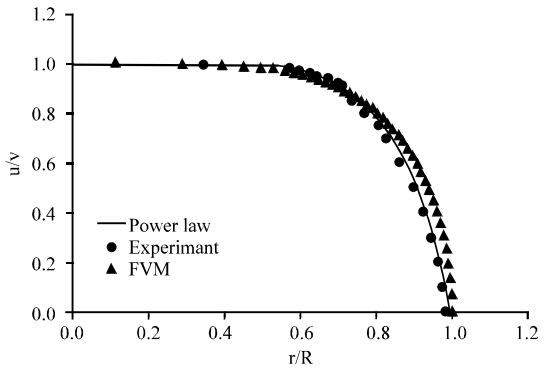

Fig. 1: Velocity profile comparison between the analytical, experimental (Nail, 1991) and FVM

Validation: First, the laminar flows was modeled with the Re numbers of 100 to study the effect of inlet velocity, boundary conditions, axial symmetry, grid independency with the axial and outlet velocity profiles as the main output for comparison with the analytical values. Then, the turbulent flows were used as the validation benchmarks.

Turbulent flow in pipe: Air flowed with the inlet velocity of 1 m/sec into a pipe with length of 20 m and diameter of 0.508 m. Reynolds number based on pipe diameter was 50,000. The standard model was chosen for turbulence modeling with standard air properties. Grid independence was also checked. The mesh sizes used in this problem were 2,100, 4,000 and 10,600 cells.

In Fig. 1, the velocity profiles obtained from the computation were very close to the benchmarked values, the differences with the theoretical power law solution $U/U_{max} = (1-r/R)^{1/n}$ where n = -1.7+1.8log (Re) had the maximum error of 3% while comparison with the experimental data (Nail, 1991) had the maximum error of 5%.

The wall $Y^+\rho U_t Y/\mu$ was a dimensionless wall unit which determine near wall region for the mesh. For viscous sub layer, the corresponding value of Y^+ was <5. For buffer layer, the Y^+ was between 5 and 30. Finally, Y^+ for log-law region was more than 30. The wall Y^+ was used to check the numerical results in addition to the velocity profile.

According to obtained results in Fig. 2, the wall Y^+ had a minimal effect on the velocity profile of the results. The values of wall Y^+ for each mesh were given in Fig. 3. It could be seen that for the 10,600 cells, $Y^+ \approx 2.5$ viscous sub layer, for 4,000 cells, $Y^+ \approx 10$ buffer region and for 2,100 meshes, $Y^+ \approx 32$ log-law region.

Flow through circular orifice: Then, the turbulent flow through a circular orifice pipe was used as the main

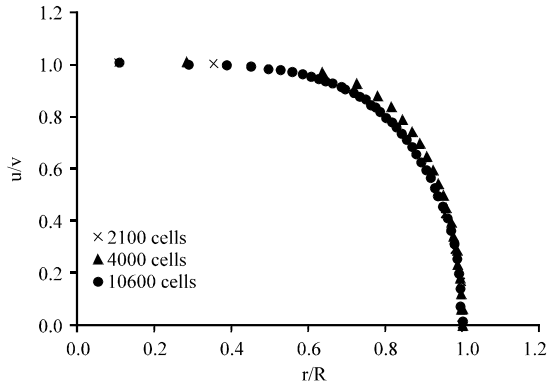

Fig. 2 Mesh effect on velocity profile

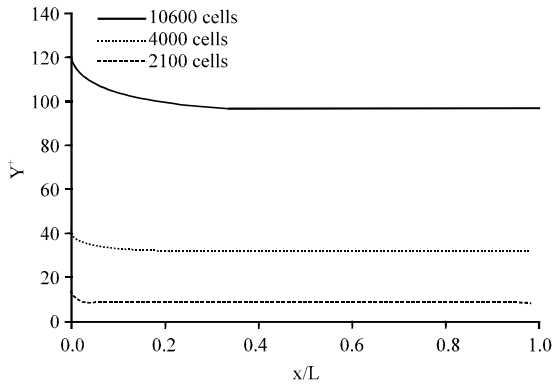

Fig. 3: Mesh effect on wall y^+

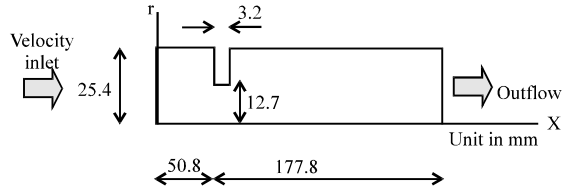

Fig. 4: Turbulent flow in circular orifice pipe geometry

validation test case. Air flowed into a pipe with a circular orifice (Nail, 1991) as shown in Fig. 4. The flow had Reynolds number of 18400, the uniform air velocity of 10.58 m/sec flows into the computational domain. Air exited to an ambient pressure of 1 atm. Standard k-ε Model was used for turbulence modeling with the air property as in the previous case.

Grid independence was also checked. The mesh sizes used in this problem were 1,500, 1,950, 3,600 and 5,700 cells. The velocity and pressure profiles for each mesh sizes were given in Fig. 5 and 6, respectively. For velocity profile, the solutions did not change when the mesh contained 3,600 or more cells. There was also no

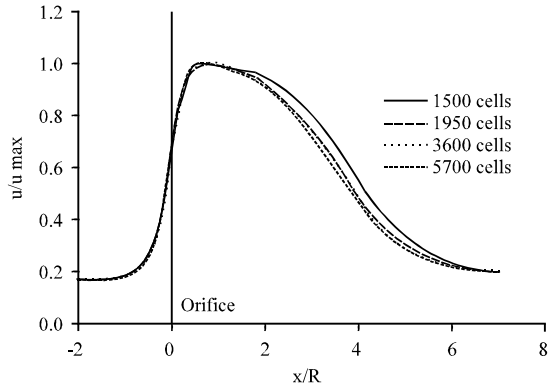

Fig. 5: Mesh effect on centerline axial velocity

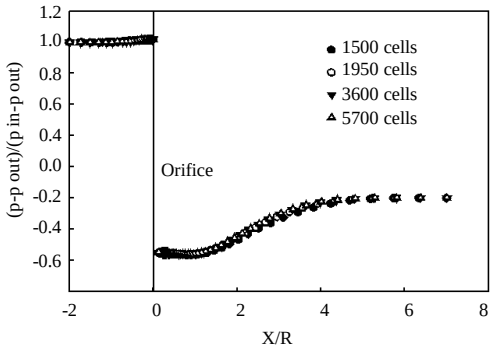

Fig. 6: Mesh effect on pressure magnitude

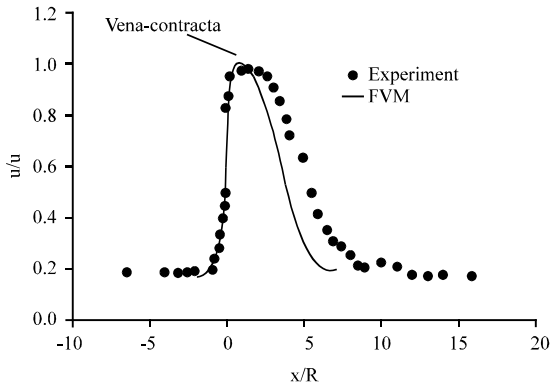

Fig. 7: Velocity comparison between the experiment (Nail, 1991) and computational results

significant change in pressure profiles. Therefore, the mesh size 3600 cells yielded grid independent results.

Centerline axial velocity for 3600 cells was compared with experimental data from (Nail, 1991) in Fig. 7. The velocity increased as it passed though the orifice until it reached the maximum value at a specific point, the vena-contracta. Beyond this point, the velocity decreased. Even though, the centerline axial velocity trend

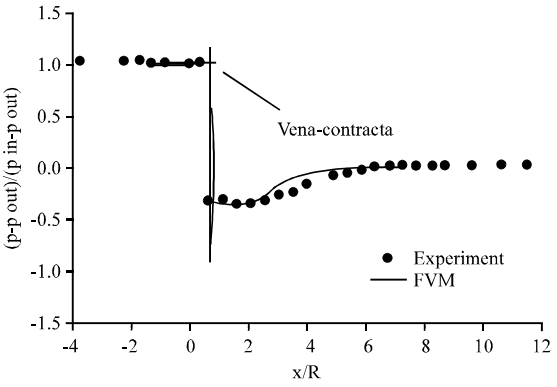

Fig. 8: Comparison of pressure between the experiment (Nail, 1991) and computational results

and vena-contracta point could be satisfactory obtained, the model cannot accurately predict the value of velocity beyond vena-contracta point.

Static pressure at the wall was also compared with experimental data (Fig. 8). The pressure decreased when the flow approached the orifice and reaches its minimum value at the vena-contracta point. Beyond this point, the pressure started to recover as the flow moves further downstream. It could be seen that standard k-ε Model failed to closely predict the pressure beyond vena-contracta point but the wall static pressure profile trend and vena-contracta point could be found.

Despite the less accurate results alfter the vena-contracta point, the obtained results still exhibited the similar shape and could be useful to predict the trend. This could be demonstrated with the value of discharge coefficient C_d which was computed from:

$$C_d = \frac{v\sqrt{1-\beta^4}}{\sqrt{2\Delta\rho s/\rho}} \quad (13)$$

The predicted value of C_d was 0.558 which was comparable to the experimental measurement at 0.610 with the error of 8%. These concluded that the accuracy was quite sufficient.

RESULTS AND DISCUSSION

Air flowed into the 2D asymmetry computational domain as illustrated in Fig. 9. The broadband noise source model was used to compute the radiated acoustic power at the end of the computational domain for 8 various values of inlet velocity: 14, 20, 28, 32, 45, 56, 68 and 75 m/sec. Air exited to ambient pressure of 1 atm. The steady state incompressible RANS equation was solved

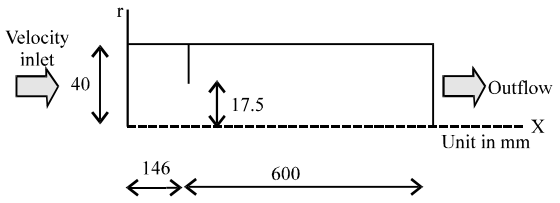

Fig. 9: Acoustic air flow though orifice pipe geometry

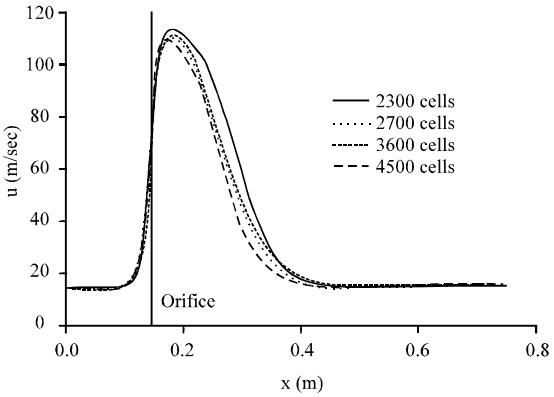

Fig. 10: Mesh effect on velocity magnitude

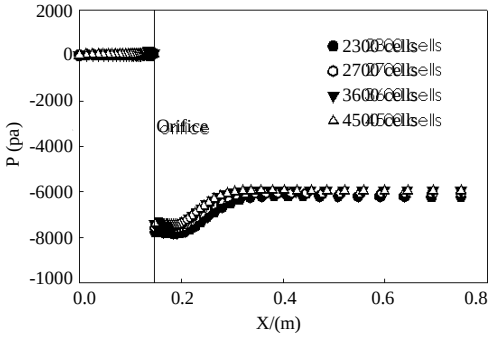

Fig. 11: Mesh effect on pressure magnitude

together with turbulence kinetic energy (Eq. 4), turbulence dissipation rate (Eq. 5) and the jet noise source model (Eq. 6). The air properties and turbulent parameters were all set to default values (Fluent, 2009).

The simple algorithm was used for pressure-velocity coupling. The second order upwind discretization scheme was used for momentum, turbulence kinetic energy and turbulence dissipation rate. Convergent criterion for each governing equations were set at 1×10^{-6}. Grid independence was checked to find the suitable mesh sizes. Four different mesh sizes were used in this simulation: 2300 cells, 2700, 3600 and 4500 cells.

Centerline axial velocity and static wall pressure profiles for each mesh sizes were given in Fig. 10 and 11, respectively. When mesh contained 3600 cells, both

Table 1: Comparison of acoustic power

	Acoustic power (dB)		
Mean velocity (m/sec)	Experiment [9]	FVM	Error (%)
14	93	72	-23
20	98	82	-16
28	102	93	-8.8
32	107	101	-5.6
45	110	109	-0.9
56	113	117	3.5
68	118	124	5.1
75	120	127	5.8

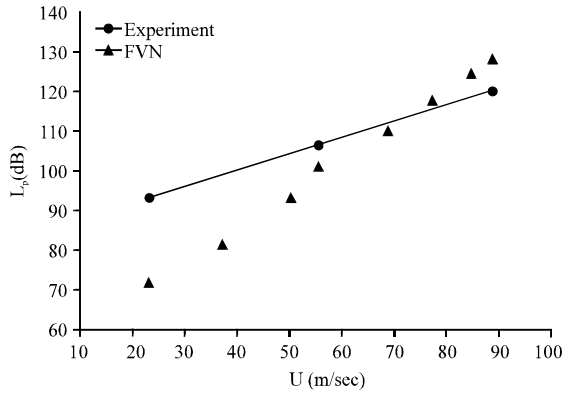

Fig. 12: Comparison of acoustic power between the experiment and the simulated results

velocity and pressure profiles were no longer changed. Thus, this mesh sufficiently gave grid independent results.

Acoustic power radiated at outlet boundary was plotted against experimental data from as shown in Table 1 and Fig. 12. The differences between numerical and experimental increased as the mean velocity decrease and then raised again.

CONCLUSION

In this research, the commercial software fluent was used to simulate flow induced noise problem. To make sure that parameters and results were accurately reliable, two benchmark problems, laminar and turbulent flows in pipes were simulated and validated against theoretical or experimental results. Good agreements were obtained for each verification case studies.

For turbulent flow through circular orifice, the problem with the k-ε Model was simulated at Re = 18400 with 4 different mesh sizes for the grid independency check. Predicted centerline axial velocity and static wall pressure profiles was plotted and compared with reliable experimental data. Results showed that standard k-ε Model failed to predict the velocity and pressure beyond vena-contracta point. However, centerline axial velocity trend, pressure profile trend and vena-contracta point could be predicted. However, when the predicted discharge coefficient was compared with experimental data, the error between numerical and experimental data was acceptable.

For the simulation of flow induced noise, the standard k-ε Model and the broadband noise source was chosen for turbulence modeling at 8 different values of air inlet velocity. The model was used to predict acoustic power radiated at the outlet boundary. Acoustic power was plotted against the mean inlet velocity. The results showed that broadband noise source model can predict acoustic power at the mean velocity range of 32-75 m/sec.

It was noted that there were some works that employed the k-ε turbulent model for flows only. However, when the accuracy of the computational results using the standard k-ε Model was considered at the low velocity range as found in snoring, there seemed to be high deviation from the experiments for the acoustic power, making the results less reliable. Hence, the next step would be the investigation of other models for instance, the Low-Reynolds-Number k-ε Model (Pirnar *et al*., 2015) or low-Re SST turbulence models (Rasani *et al*., 2011a, b). The change of acoustic model was also considered.

REFERENCES

Fluent, A., 2009. Ansys Fluent 12.0 Tutorial Guide. Ansys Inc, Canonsburg, Pennsylvania,.

Goldstein, M. and B. Rosenbaum, 1973. Effect of anisotropic turbulence on aerodynamic noise. J. Acoust. Soc. Am., 54: 630-645.

Jennum, P. and A. Sjol, 1993. Snoring, sleep apnoea and cardiovascular risk factors: The MONICA II study. Int. J. Epidemiol., 22: 439-444.

Liu, Z.S., X.Y. Luo, H.P. Lee and C. Lu, 2007. Snoring source identification and snoring noise prediction. J. Biomech., 40: 861-870.

Mihaescu, M., S. Murugappan, E. Gutmark, L.F. Donnelly and M. Kalra, 2008. Computational modeling of upper airway before and after adenotonsillectomy for obstructive sleep apnea. Laryngoscope, 118: 360-362.

Nail, G.H., 1991. A study of 3-dimensional flow through orifice meter. Ph.D Thesis, Texas A and M University, Texas, USA.

Rasani, M.R., K. Inthavong and J.Y. Tu, 2011a. Simulation of pharyngeal airway interaction with air flow using low-re turbulence model. Modell. Simul. Eng., 2011: 1-9.

Rasani, M.R., K. Inthavong and J.Y. Tu, 2011b. Three-dimensional fluid-structure interaction modeling of expiratory flow in the pharyngeal airway. In: Proceedings of the 5th Kuala Lumpur Internat ional Conference on Biomedical Engineering, June 20-23, 2011, Springer, Berlin, Germany, ISBN: 978-3-642-21728-9, pp: 467-471.

Sarasaen, C., K. Hemtiwakorn, T. Bhongmakapat, J. Laothamatas and C. Pintavirooj, 2012. Computational Fluid Dynamic (CFD) in thai patient with Obstructive Sleep Apnea Syndrome (OSAS) a case report: Comparative study between healthy and OSA subject. Proceedings of the 2012 International Conference on Biomedical Engineering, (BMEiCON), December 5-7, 2012, IEEE, Bangkok, Thailand, ISBN:978-1-4673-4890-4, pp: 1-6.

Shah, M.S., J.B. Joshi, A.S. Kalsi, C.S.R. Prasad and D.S. Shukla, 2012. Analysis of flow through an orifice meter: CFD simulation. Chem. Eng. Sci.,71: 300-309.

Wexler, D., R. Segal and J. Kimbell, 2005. Aerodynamic effects of inferior turbinate reduction: Computational fluid dynamics simulation. Arch. Otolaryngology Head Neck Surg., 131: 1102-1107.